Dalton Transactions

ROYAL SOCIETY OF CHEMISTRY

PAPER

View Article Online
View Journal | View Issue

Cite this: *Dalton Trans.*, 2025, **54**, 10657

Dose-dependent gamma irradiation effects on Ni nanoparticle size in rGO–Ni nanocomposites for enhanced electrochemical performance

Raynara M. S. Jacovone, [a] Miguel Duarte, [a] Jaqueline J. S. Soares, [a] Rubens N. Faria, [a] Rafael H. L. Garcia, [a] Lucio Angnes [b] and Solange K. Sakata *[a]

Received 2nd August 2024,
Accepted 16th June 2025

DOI: 10.1039/d4dt02211d

rsc.li/dalton

This study introduces an environmentally friendly method for synthesizing reduced graphene oxide/nickel (rGO–Ni) nanocomposites for electrochemical applications using gamma irradiation. This approach eliminates the need for toxic chemical reductants and mitigates the generation of hazardous residues and undesirable by-products. The effect of the gamma irradiation dose on the size of nickel nanoparticles supported on graphene oxide was also investigated. The graphene oxide (GO) dispersion was subjected to gamma irradiation in the presence of the $(Ni[(NH_3)_6]Cl_2)$ complex at doses of 20, 40 and 80 kGy and a dose rate of 10 kGy h^{-1}. X-ray diffraction confirmed the formation of metallic Ni and the simultaneous reduction of graphene oxide (GO) induced by gamma irradiation, while X-ray photoelectron spectroscopy indicated the oxidation of the Ni metal on the GO surface. These findings were further corroborated by thermogravimetric analysis. To evaluate the electrochemical properties, screen-printed electrodes were modified with rGO and rGO–Ni. Cyclic voltammetry measurements in the presence of $K_3[Fe(CN)_6]$ demonstrated reversible redox behavior for all samples. It is noteworthy that rGO–Ni/SPE exhibited a significant enhancement in the anodic peak currents (I_{pa}) and electroactive surface area compared to the unmodified SPE. Furthermore, a direct correlation was observed between the I_{pa} value and the gamma radiation dose applied during the nanocomposite synthesis. These results point out the potential applications of rGO–Ni nanocomposites in electrochemical devices.

1. Introduction

The functionalization of reduced graphene oxide (rGO) with metal nanoparticles (NPs) has proven to be an effective approach for enhancing its properties and expanding its applications by stabilizing nanoparticles and preventing their aggregation and oxidation.[1] Among metal nanoparticles, nickel (Ni) has shown significant synergistic effects with rGO, improving conductivity.[2] The rGO–Ni nanocomposite exhibits excellent potential for various electronic applications such as sensors/biosensors, catalysts, hydrogen production/storage, and, particularly, supercapacitors.[3,4]

Although rGO/Ni NP-based materials have been reported for use in electronic devices, achieving high electrochemical performance remains a challenge due to issues such as agglomeration of reduced graphene oxide sheets and non-homogeneous coating of nickel nanoparticles onto the rGO surface.[5,6] The method used for synthesizing the nanocomposite plays a crucial role in determining its electronic performance.

Various synthetic routes have been reported to produce rGO–Ni nanocomposites, with chemical reduction and thermal reduction being the most commonly used methods.[7,8] However, most of these techniques involve disadvantages such as using toxic chemical reductants, extended reaction time, and high-temperature treatment, which limit the scalability of rGO–Ni production. In contrast, gamma irradiation synthesis offers an environmentally friendly alternative for producing rGO and its nanocomposites. This method is conducted at room temperature in an aqueous solution, without toxic reagents or the generation of undesirable by-products, implying that no further purification is required.[9,10]

Despite the potential advantages of the gamma radiation technique, only two studies have reported its use for rGO–Ni synthesis. Furthermore, these studies specifically focused on

[a]*Nuclear and Energy Research Institute, National Commission of Nuclear Energy (IPEN/CNEN - SP), Av. Prof. Lineu Prestes 2242, 05508-000, São Paulo, SP, Brazil. E-mail: sksakata@ipen.br*
[b]*Department of Fundamental Chemistry, Institute of Chemistry, University of São Paulo, Av. Prof. Lineu Prestes 748, 05508-000, São Paulo, SP, Brazil*

investigating the electromagnetic absorption of the rGO–Ni nanocomposite.[11,12] By addressing the limitations observed in earlier studies and exploring the advantages offered by gamma irradiation synthesis, our study aims to elucidate the correlation between the absorbed dose and the size of Ni nanoparticles on rGO. Additionally, we investigate the impact of these factors on the electrochemical properties of the nanocomposite for application in advanced electronic devices.

2. Experimental

All the chemicals used in this study are of analytical grade and were used without further purification. Deionized water was used to prepare all solutions. Graphite powder (99% purity) and $NaNO_3$ were purchased from Merck; $KMnO_4$, NaOH, $NiCl_2{\cdot}6H_2O$, H_2SO_4, and HCl were acquired from Labsynth (Brazil); and isopropyl alcohol (C_3H_7OH), dimethylformamide (DMF) and 30% H_2O_2 were obtained from Sigma-Aldrich.

2.1. Synthesis of graphene oxide (GO)

Graphene oxide was synthesized using a modified Hummers' method.[13] Briefly, 3 g of graphite powder, 3 g of $NaNO_3$ and 140 mL of H_2SO_4 were mixed and stirred in an ice bath. Following that, 18 g of $KMnO_4$ was slowly added to the mixture, maintaining a temperature of approximately 35 °C for one hour. Then, 100 mL of deionized (DI) water was added and the solution was stirred at 90 °C. Finally, an additional 100 mL of DI water was added to the solution along with 18 mL of H_2O_2 (30%), which changed the color from dark brown to yellow. The resulting mixture was centrifuged at 12 000 rpm for 10 minutes, and the obtained product was washed with DI water and NaOH [1.0 M] until reaching a pH of 7, followed by HCl [1.0 M] until the pH was around 5. GO was dispersed in water, exfoliated in an ice bath using ultrasonic equipment for 20 minutes and then freeze-dried for further characterization.

2.2. Synthesis of rGO and rGO–Ni nanocomposites

For the reduction of GO, 10 mL of re-dispersed GO (2 mg mL^{-1}) in a 1 : 1 water/isopropanol mixture[14] was transferred into 20 mL Wheaton '180'® low-potassium borosilicate glass vials. The mixture was purged with nitrogen gas to remove dissolved oxygen and subsequently subjected to gamma irradiation. The sealed vials were irradiated using a ^{60}Co source at the Multipurpose Gamma Facility, Nuclear and Energy Research Institute (IPEN/CNEN-SP, Brazil), with doses ranging from 20 to 80 kGy and a dose rate of 10 kGy h^{-1} at *ca.* 34–38 °C. The resulting product was washed with DI water and centrifuged at 13 000 rpm for 20 minutes. Finally, the obtained reduced graphene oxide was freeze dried for further characterization.

For the rGO–Ni nanocomposite synthesis, 20 mmol of Ni $[(NH_3)_6]Cl_2$ complex was slowly added to the re-dispersed GO (2 mg mL^{-1}) in a water/isopropanol (1 : 1) mixture, resulting in a 5 mM solution of Ni^{2+}. The mixture was purged with nitrogen gas, followed by gamma irradiation, using the same protocol applied for rGO. The dose was measured using PMMA (polymethyl methacrylate) dosimeters of the red type.

2.3. Characterization techniques

The morphology of samples was characterized by transmission electron microscopy (TEM) using a JEOL instrument, model JEM-2100, at 200 kV acceleration voltages. The size distribution was calculated using ImageJ software. X-ray diffraction (XRD) measurements were performed on a Bruker D8 ADVANCE equipped with a copper tube and scintillation detector, with counting times of 6 seconds per step size of 0.05°. Raman spectra were acquired using a Horiba XploRA PLUS raman spectrometer with a 785 nm laser. X-ray photoelectron spectroscopy (XPS) spectra were recorded on a Thermo Scientific instrument, model K-alpha, and thermogravimetric analyses (TGA) were performed using an SDTQ 600 (TA Instruments) thermal analyzer over a temperature range of 50 °C to 800 °C, with a heating rate of 10 °C min^{-1} under an air flow of 50 mL min^{-1}.

2.4. Electrochemical measurements

The electrochemical behavior of rGO and rGO–Ni was assessed by cyclic voltammetry (CV) using a portable potentiostat (Metrohm, model 910 PSTAT mini) and PSTAT Software 1.0 for data acquisition. The measurements were carried out using a screen-printed electrode (SPE) from Metrohm, model 6.1208.110. Carbon was used as the working and counter electrodes and silver as the reference electrode. The working electrode surface was modified using the drop casting method as follows: the nanomaterial was dispersed in DMF at a concentration of 10 mg mL^{-1} using an ultrasonic bath for 30 minutes, and 5 μL of the dispersed mixture was applied to the working electrode and dried at room temperature. The modified SPEs are referred to in this paper as rGO40/SPE, rGO80/SPE, rGO–Ni40/SPE, and rGO–Ni80/SPE.

3. Results and discussion

3.1. The effect of gamma irradiation on rGO/Ni preparation

Gamma irradiation induces water radiolysis generating reducing species:[15] hydrogen radicals and solvated electrons, e^-_{aq} (eqn (1)):

$$H_2O\ \gamma\text{-irradiation} \rightarrow e_{aq}^- + H^\bullet + HO^\bullet \quad (1)$$

In the radiolysis process, a highly oxidizing species, the radical hydroxyl ($HO^\bullet$), is also formed. To prevent oxidation, isopropyl alcohol was added to the mixture to scavenge $HO^\bullet$ radicals (as shown in eqn (2)):

$$(CH_3)_2CHOH + HO^\bullet \rightarrow (CH_3)_2C^\bullet OH + H_2O \quad (2)$$

The e^-_{aq} and $H^\bullet$ species have a reductive potential, $E°$, of −2.9 V and −2.4 V, respectively. They are capable of reducing oxygen-containing functional groups present in the GO sheets and converting Ni^{2+} into a zero valence state, $E°$ (Ni^{2+}/Ni^0 =

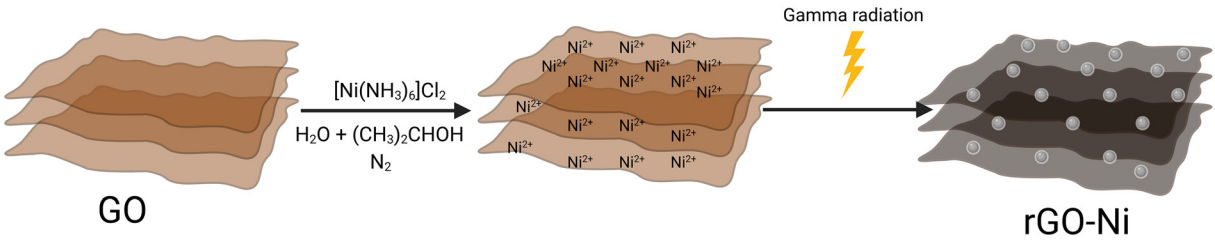

Fig. 1 Schematic representation of the synthesis of rGO–Ni nanocomposites using gamma irradiation.

−0.24 V),[9] as described in eqn (3) and (4), and therefore, gamma radiation simultaneously reduces GO and Ni^{2+}, to produce the rGO–Ni nanocomposite (Fig. 1).

$$Ni^{2+} + 2e^{-}_{aq} \rightarrow Ni^{0} \quad (3)$$

$$Ni^{2+} + 2H^{\bullet} \rightarrow Ni^{0} + 2H^{+} \quad (4)$$

3.2. Physicochemical properties of GO and the rGO–Ni nanocomposite

Raman spectroscopy was employed to analyze the reduction of graphene oxide, as shown in Fig. 2. The graphene oxide spectrum exhibited two bands attributed to graphene-based materials: the D band, located at approximately 1317 cm^{-1}, indicating induced disorder, and the G band, around 1585 cm^{-1}.[16] Additionally, the I_D/I_G ratio, indicative of surface defects in carbon materials, was calculated.

Compared to GO, which had an I_D/I_G ratio of 1.9, all nanocomposite samples showed higher I_D/I_G values, 2.0, 2.1 and 2.4, for rGO–Ni20, rGO–Ni40 and rGO–Ni80, respectively, indicating that the reduction process increases the formation of defect sites on the GO surface.

The morphologies and structures were determined using TEM (Fig. 3). The micrograph of GO (Fig. 3a) revealed typical sheet-like 2D structures, while the images in Fig. 3b–d of the rGO–Ni20, rGO–Ni40, and rGO–Ni80 showed NiNPs. These analysies confirm the successful reduction of nickel ions by gamma irradiation.

TEM analyses also revealed a correlation between radiation dose and the size distribution of NiNPs supported on rGO. At the lowest absorbed dose (20 kGy, Fig. 3b), significant agglomeration of NiNPs on the rGO sheets was observed. This occurs because, at low doses, the concentration of metallic ions exceeds that of their reduced form, promoting agglomeration.[17] Due to this effect, the nanocomposite obtained at 20 kGy was excluded from further study.

The average size of Ni nanoparticles decreased from 12 nm at 40 kGy to 4 nm at 80 kGy doses, indicating that a higher dose promotes the formation of smaller nanoparticles. The observed decrease in nanoparticle size can be attributed to the non-linear dynamics of nanoparticle formation. Small, unstable nanoparticles may redissolve due to high surface energy and solubility, facilitating the growth of larger, stable particles *via* a process known as Ostwald ripening.[18] This process occurs because particles must exceed a critical radius

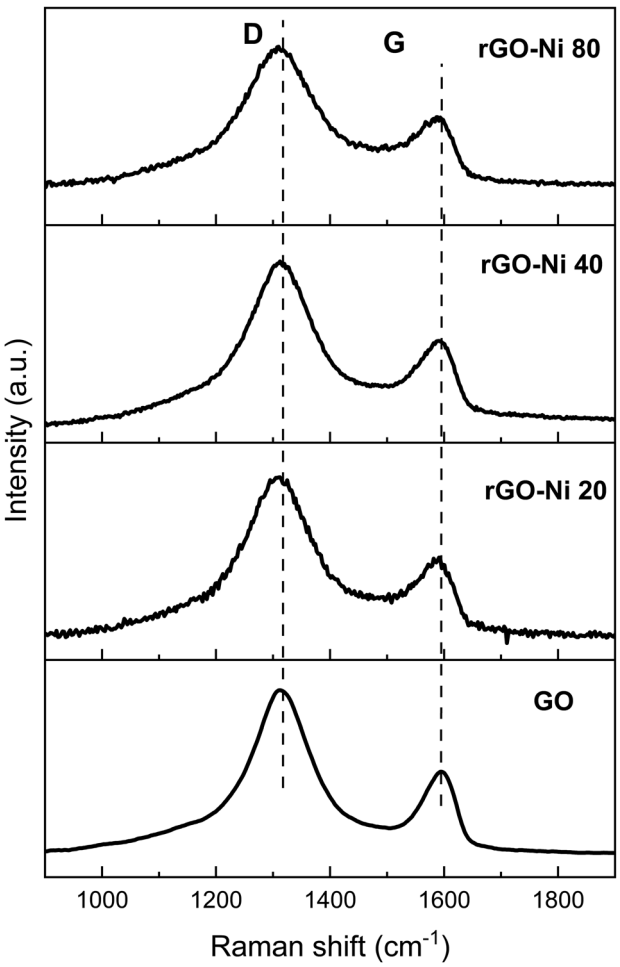

Fig. 2 Raman spectra of GO, rGO–Ni20, rGO–Ni40 and rGO–Ni80.

to achieve thermodynamic stability and reach equilibrium with the solution.[19] In our study, at 40 kGy, the results suggested that many small nuclei did not reach this critical radius and redissolved, leading to the growth of larger particles. In contrast, irradiation at 80 kGy allowed more nuclei to reach the critical size, resulting in a higher number of stable nanoparticles. As the initial nickel concentration remained constant, more growing nuclei increased competition for available nickel, yielding smaller nanoparticles.

The chemical compositions, bonding configurations before and after GO irradiation and the Ni content on the

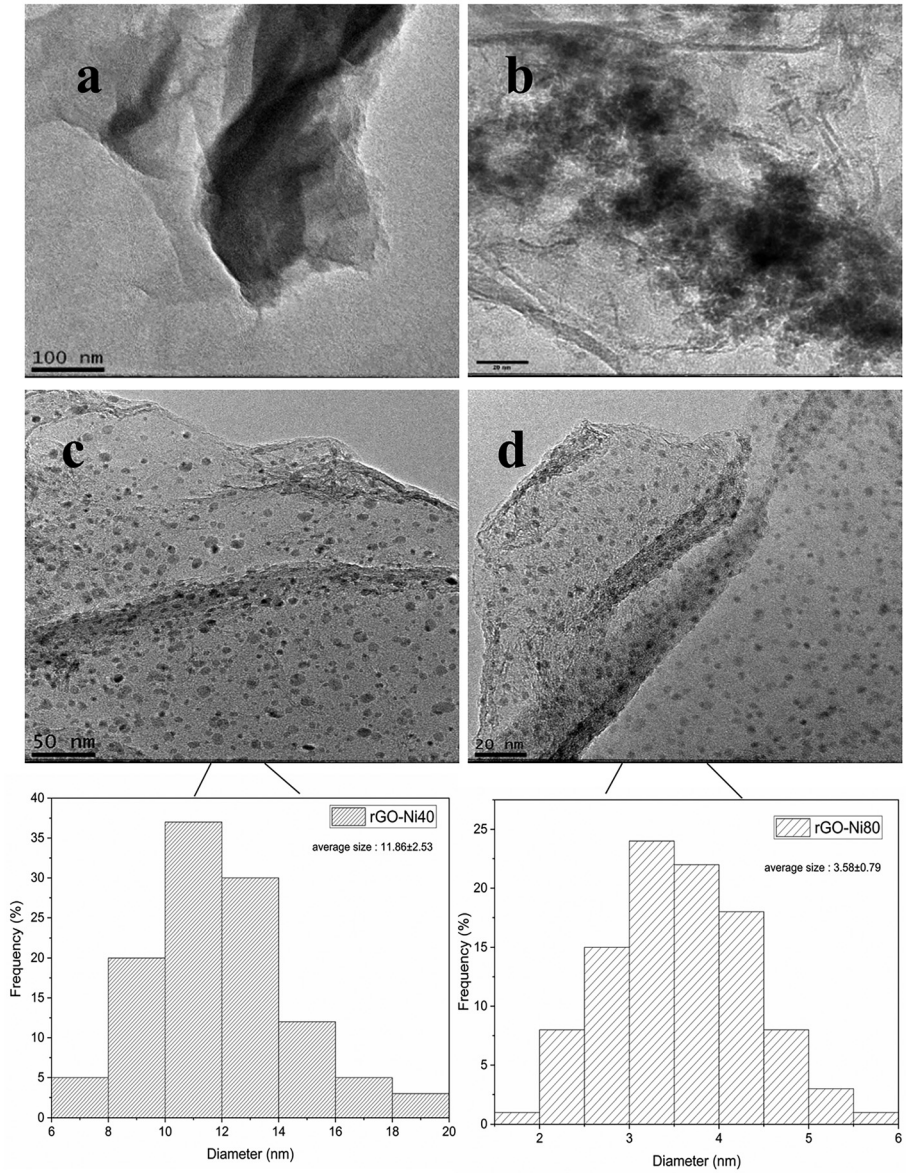

Fig. 3 TEM characterization of GO (a), rGO–Ni20 (b), rGO–Ni40 (c) and rGO–Ni80 (d) and the histogram of size distribution of Ni nanoparticles supported on rGO. The Ni particles appear dark in the image due to the higher atomic number of Ni (Z = 28) compared to carbon atoms (Z = 6), have a spherical shape and are well dispersed on rGO sheets.

nanocomposite surface were characterized using (XPS). The survey spectra are presented in Fig. 4a; the spectra show two peaks corresponding to the binding energies at 285 eV and 532 eV, corresponding to C 1s and O 1s, respectively. Additionally, in the nanocomposites, peaks located around 68 eV, 113 eV, 856 eV, and 874 eV correspond to Ni 3p, Ni 3s, Ni $2p_{3/2}$, and Ni $2p_{1/2}$ respectively.[6,20]

The high-resolution XPS spectra of C 1s are presented in Fig. 4b. All spectra exhibit four main peaks at 284.5, 286.5, 287.7, and 288.5 eV, attributed to C–C, C–OH, C═O, and O–C═O bonds, respectively.[5] As shown in Fig. 4c, the O 1s spectra of GO and the rGO–Ni samples display a peak around 532 eV, which is attributed to residual oxygen functional groups such as hydroxyl and carbonyl resulting from the reduction process. However, in all nanocomposite samples, a peak at 531.5 eV emerged, corresponding to the Ni–O bond. The Ni 2p spectra (Fig. 4d) were deconvoluted into four distinct peaks: 855.5 eV and 873.5 eV, corresponding to Ni $2p_{3/2}$ and Ni $2p_{1/2}$ of NiO, and 861.3 eV and 880.2 eV, attributed to their satellite peaks. These findings indicate the formation of nickel oxide, likely resulting from the oxidation of metal nickel species on the rGO surface.[21,22]

Table 1 shows that the C/O ratio increased from 2.5 to 4.4 as the radiation dose increased, indicating the gradual reduction of graphene oxide and the amount of Ni nano-

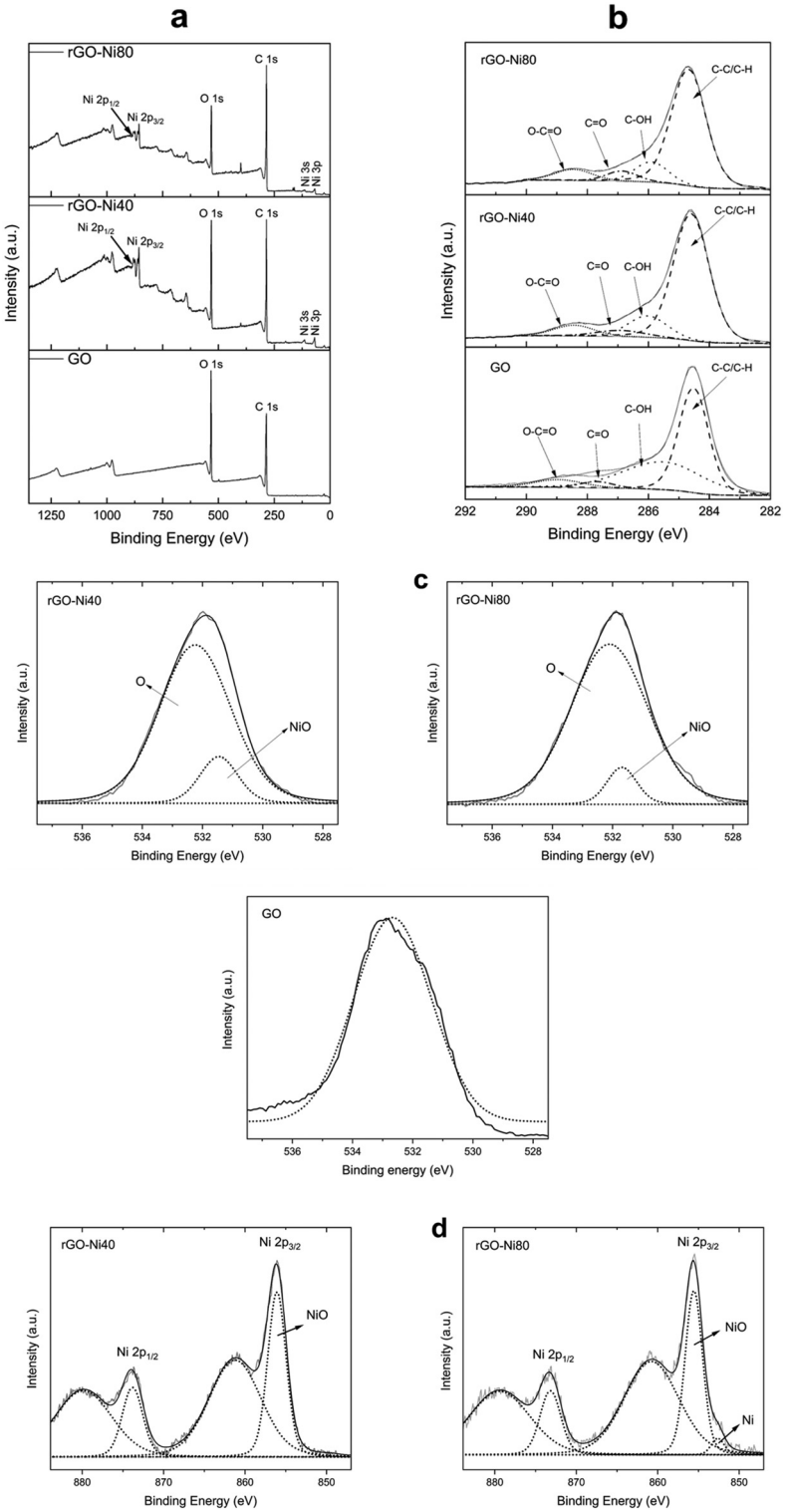

Fig. 4 (a) X-ray photoelectron spectroscopy survey spectra; (b) XPS high-resolution C 1s spectra of rGO–Ni80, rGO–Ni40 and GO; (c) XPS high resolution O 1s spectra of rGO–Ni40 and rGO–Ni80; and (d) XPS high resolution Ni 2p spectra of rGO–Ni40 and rGO–Ni80.

particles on the rGO surface, as determined by XPS analysis.

Table 2 shows the atomic percentage contributions of each functional group. After reduction, the percentages of Ni–O and C–C/C–H bonds increased as a function of the applied irradiation dose. On the other hand, the area peaks for C–OH and C═O decreased by nearly 50% for rGO–Ni80 compared to GO.

Table 1 Elemental atomic content (at%) of GO, rGO–Ni40 and rGO–Ni80 calculated from the respective survey XPS spectra

Sample	C (%)	O (%)	Ni (%)	C/O
GO	71.7	28.3	0	2.5
rGO–Ni40	76.0	21.3	2.6	3.6
rGO–Ni80	79.0	18.1	2.9	4.4

Table 2 Percentage abundance of different bonds based on the area of the respective fitted high resolution XPS peaks of the samples at different absorbed doses

Sample	C–C/C–H (C 1s)	C–OH (C 1s)	C═O (C 1s)	O–C═O (C 1s)	Ni–O (O 1s)	NiO (Ni 2p)	Ni (Ni 2p)
GO	58.8	21.1	12.6	7.5	—	—	—
rGO–Ni40	74.0	13.7	5.1	7.2	13.5	99.8	—
rGO–Ni80	75.4	12.3	5.3	7.0	8.2	93.8	6.2

XRD analysis enables monitoring the graphene oxide reduction process. Fig. 5 shows the XRD patterns of GO, rGO-40, rGO-80, rGO–Ni40 and rGO–Ni80.

The characteristic GO peak (001) located at 11.1° shifted to a larger angle, around 24°, and decreased in intensity for all irradiated samples, indicating the formation of rGO. Furthermore, the peaks observed at 44.5° and 51.8° align with the (111) and (200) planes of face-centered cubic (fcc) metallic Ni crystals (COD no. 2100658). The diffractogram validates the simultaneous reduction of GO and Ni^{2+} during the gamma radiation synthesis.[11,12] As no peaks related to NiO were observed in XDR analysis, the results suggest that metallic Ni nanoparticles are located mainly between the rGO layers, while the NiO detected in the XPS analysis formed through air oxidation on the rGO surface.

Although the conversion of GO into rGO cannot be entirely quantitative due to competing reduction processes involving both GO and Ni^{2+}, TGA was conducted under an air atmosphere to oxidize Ni^0 and determine the mass percentage of NiNPs within rGO as the residue NiO. Fig. 6 presents two TGA curves: reduced graphene oxide with nickel (rGO–Ni80) and GO, for comparison purposes.

TGA curves depict mass loss as a function of temperature, with the first derivative (DTGA) of GO revealing a significant mass loss near 100 °C, attributed to the desorption of surface water. A gradual mass loss observed between 200 °C and 300 °C is associated with the pyrolysis of hydroxyl, epoxy, and carboxyl groups.[23] For GO, the mass loss between 500 °C and 600 °C corresponds to the combustion of carbon backbones, whereas for rGO–Ni, the residual mass percentage is attributed to the presence of nickel, incorporated into the reduced graphene oxide in the form of nickel oxide. Table 3 summarizes the percentage of mass loss for GO, rGO–Ni 40 and rGONi80.

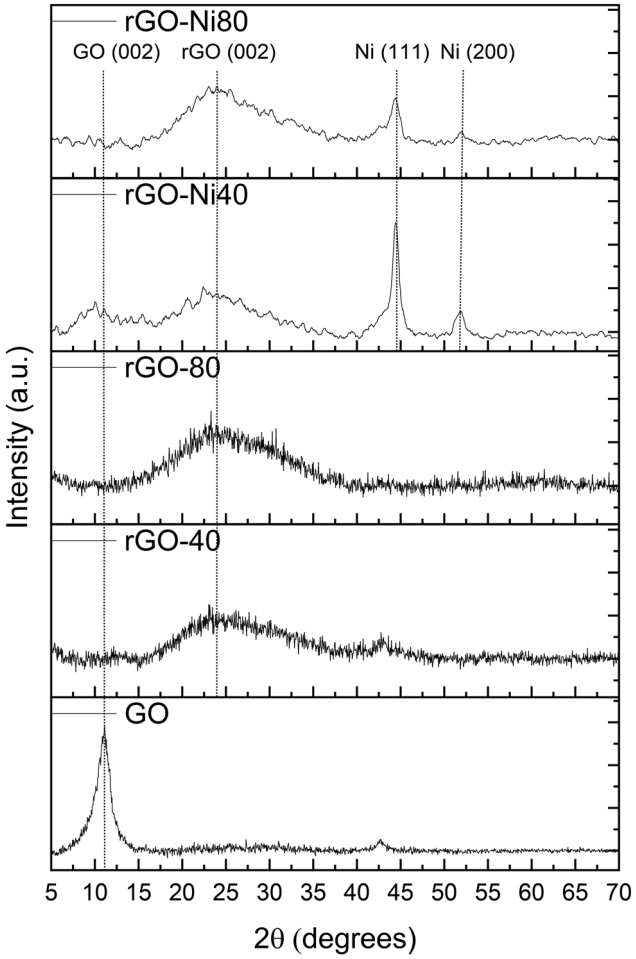

Fig. 5 XRD patterns of GO, rGO-40, rGO-80, rGO–Ni40 and rGO–Ni80.

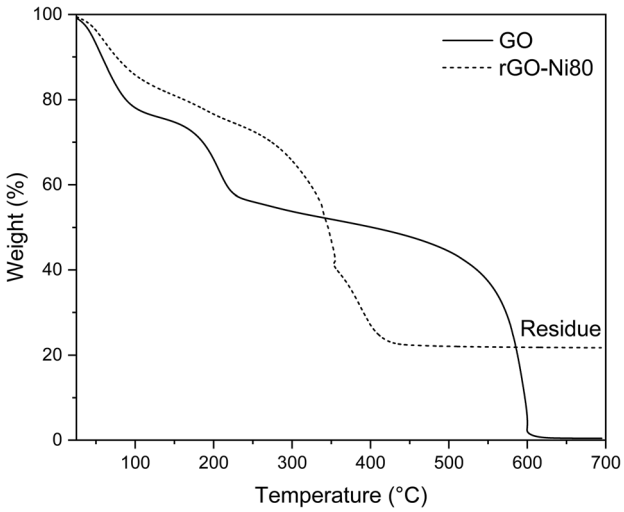

Fig. 6 Comparison between the TGA curves of graphene oxide and reduced graphene oxide–nickel under an air atmosphere.

Table 3 Elemental atomic content (at%) of GO, rGO–Ni40 and rGO–Ni80 calculated from TGA

Sample	Carbon backbone (%)	Oxygen groups (%)	Residue (NiO) (%)	C/O
GO	72.5	27.5	—	2.6
rGO–Ni40	58.5	16.7	24.8	3.5
rGO–Ni80	60.0	14.2	25.8	4.2

3.3. Electrochemical properties – cyclic voltammetry studies

SPE were modified using the drop-casting method with rGO and rGO–Ni dispersions. These nanomaterials exhibited excellent stability in dimethylformamide (DMF).[24] The electrochemical response of both the SPE and the SPE modified with rGO in the presence of $K_3[Fe(CN)_6]$ is shown in Fig. 7. The shape of the curves indicates a reversible system for all the samples.

However, significant differences were observed in both the peak anodic (I_{pa}) and cathodic (I_{pc}) currents, along with the peak anodic (E_{pa}) and cathodic (E_{pc}) potentials. An increase in both I_{pa} and I_{pc} was noted as absorbed doses increased (Table 4).

At the unmodified SPE, the I_{pa} was 51 μA, while at rGO80/SPE, it measured 80 μA, marking a significant 78% increase in this parameter. This emphasizes the significant enhancement in the electrical conductivity of the SPE achieved through modification with rGO synthesized using gamma radiation.

Additionally, all rGO/SPE samples exhibited a smaller ΔE ($E_{pa} - E_{pc}$) compared to the unmodified SPE (Table 5), indicating an improvement in electron transfer on the modified electrode's surface due to the restoration of a graphitic network of sp^2 bonds during the reduction process.[24,25]

Table 4 Comparison between I_{pa} values of electrodes modified with rGO/SPE and rGO–Ni/SPE

Sample	I_{pa} (μA)	Sample	I_{pa} (μA)
rGO40/SPE	68 ± 1.1	rGO–Ni40/SPE	80 ± 2.9
rGO80/SPE	80 ± 1.2	rGO–Ni80/SPE	83 ± 4.2

Table 5 I_{pa}, I_{pc} and ΔE parameters for the bare SPE, rGO40/SPE and rGO80/SPE

Sample	I_{pa} (μA)	I_{pc} (μA)	ΔE_p (mV)
SPE	51	−33	740
rGO40/SPE	68	−56	620
rGO80/SPE	80	−69	280

The average electroactive area for both the bare SPE and the rGO-modified SPE was determined using the Randles–Sevcik formula (eqn (5)):

$$I_{pa} = 2.7 \times 10^5 n^{3/2} A D_o^{1/2} C_o v^{1/2}$$
$$D_o = 6.3 \times 10^{-6}\ \mathrm{cm^2\ s^{-1}} \quad (5)$$

where I_{pa} refers to the anodic peak current (A), n stands for the electron transfer number, A denotes the surface area of the electrode (cm^2), D_o indicates the diffusion coefficient ($cm^2\ s^{-1}$),[25] C_o represents the concentration of $K_3[Fe(CN)_6]$ (mol L^{-1}), and V refers to the scan rate (V s^{-1}).

The electroactive area values obtained for the bare SPE, rGO40/SPE, and rGO80/SPE were 0.080 cm^2, 0.112 cm^2 and 0.132 cm^2, respectively, indicating a substantial increase in the effective surface area of the electrode due to the presence of rGO.

Fig. 8 illustrates the electrochemical behavior of the investigated nanocomposites, rGO/Ni, under two different absorbed

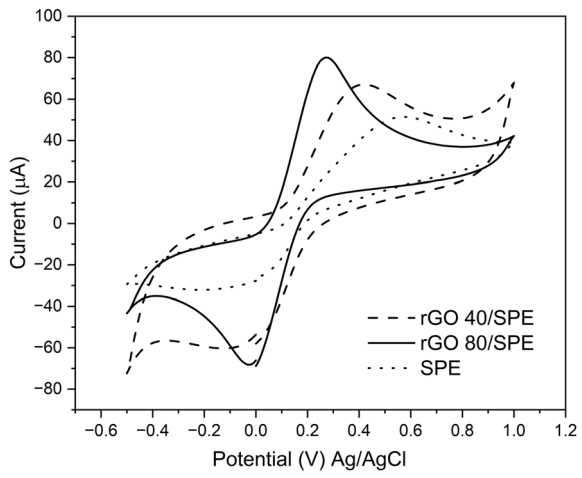

Fig. 7 Cyclic voltammograms obtained for 4 mmol L^{-1} $K_3[Fe(CN)_6]$ in 0.05 mol L^{-1} KCl at a scan rate of 50 mV s^{-1} using the bare SPE and the SPE modified with rGO 40 kGy and rGO 80 kGy.

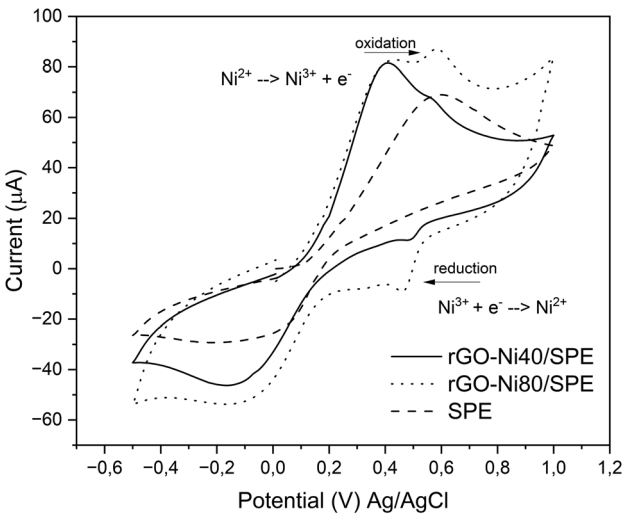

Fig. 8 Cyclic voltammograms obtained for 4 mmol L^{-1} $K_3[Fe(CN)_6]$ in 0.05 mol L^{-1} KCl at a scan rate of 50 mV s^{-1} using the SPE modified with rGO–Ni40 and rGO–Ni80.

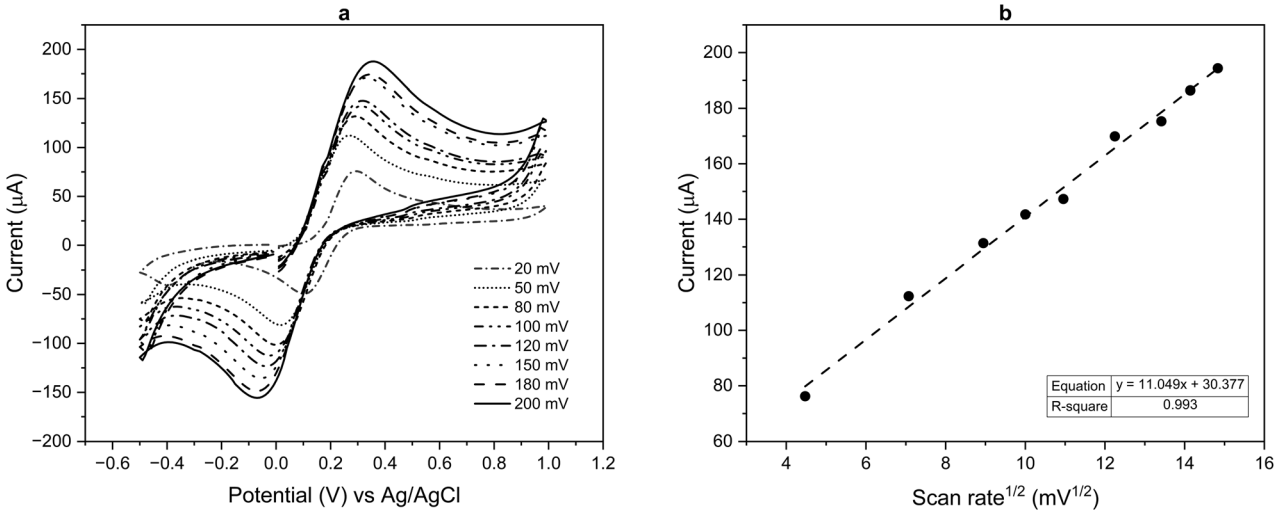

Fig. 9 Cyclic voltammograms recorded for rGO–Ni80/SPE (a) and the correlation between the anodic current (μA) and the scan rate$^{1/2}$ (mV s^{-1})$^{1/2}$ of rGO–Ni80/SPE measured in 4 mmol L^{-1} $K_3[Fe(CN)_6]$ at different scan rates (20–200 mV s^{-1}) (b).

doses. CV curve of rGO/Ni80 demonstrated the presence of two pairs of anodic and cathodic peak potentials at 390 and 135 mV (attributed to Fe^{3+}/Fe^{2+}), and 580 and 470 mV (attributed to Ni^{3+}/Ni^{2+}), indicating the presence of nickel nanoparticles on the electrode surface.[26]

The electrochemical performance of the rGO–Ni nanocomposite was primarily determined by the amount and accessibility of active sites, which may include oxygen-containing functional groups on the reduced graphene oxide sheets, structural defects, and the incorporated Ni nanoparticles, all of which contribute to redox reactions and facilitate charge transfer processes. The increased concentration of Ni nanoparticles, induced by gamma irradiation at 80 kGy, may have led to the saturation of available active sites on the rGO surface, resulting in a less pronounced enhancement of the anodic peak current. This could explain why the improvement in I_{pa} for rGO/rGO–Ni80 was not as significant compared to the other studied nanocomposites.

The cyclic voltammograms indicated a slightly higher anodic peak current (Table 4), compared to rGO/SPE, due to the synergistic effects between rGO and NiNPs, enhancing electrode conductivity. Furthermore, the calculated average electroactive area values for rGO–Ni40/SPE and rGO–Ni80/SPE were determined to be 0.132 cm^2 and 0.137 cm^2, respectively. These values are significantly higher than that of the bare SPE and slightly higher than that of the corresponding rGO/SPE.

The influence of different scan rates, ranging from 20 to 200 mV s^{-1}, on rGO–Ni80/SPE was evaluated in a solution con-

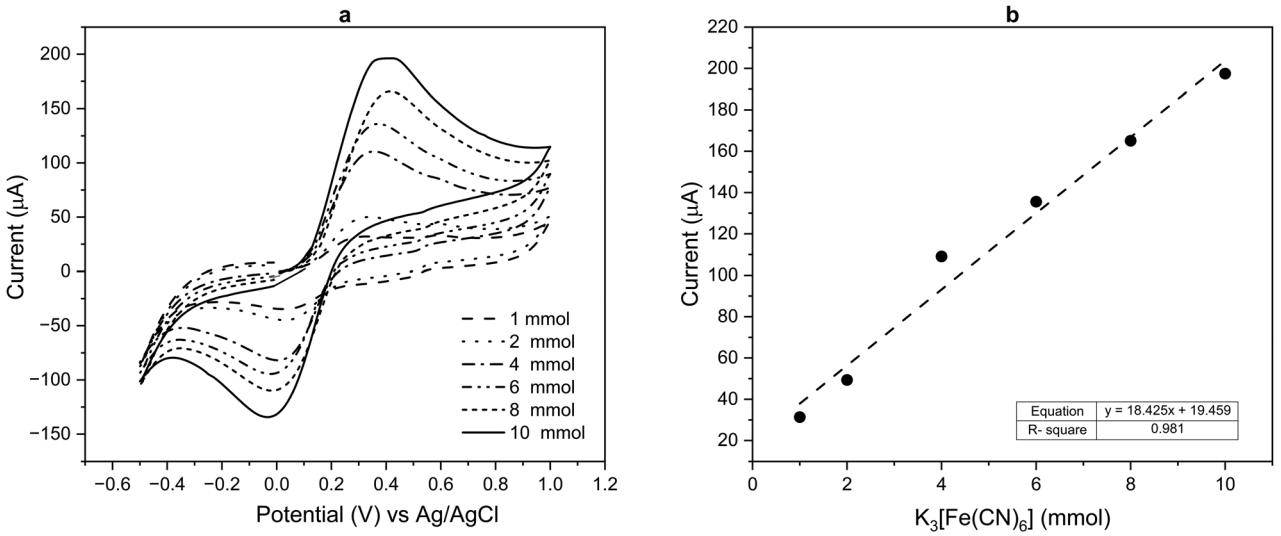

Fig. 10 Cyclic voltammograms of rGO–Ni80/SPE (a) and the correlation between anodic current (μA) and different $K_3[Fe(CN)_6]$ concentrations (1–10 mmol) at a scan rate of 50 mV s^{-1} (b).

taining 4 mmol of $K_3[(FeCN_6)]$ (Fig. 9a). A direct correlation between the scan rate and increasing current was observed, revealing a linear relationship (R^2 = 0.993), as illustrated in Fig. 9b.

The effect of concentration (ranging from 1 to 10 mmol) was also investigated and is presented in Fig. 10a.

The results demonstrated that increasing the concentration of $K_3[(FeCN_6)]$ led to a linear increase in the par-redox current amplitude (R^2 = 0.981, Fig. 10b), indicating a diffusional process.[27,28]

All reported electrochemical parameters showed that rGO–Ni80 exhibits the necessary surface structure and electronic properties to facilitate a rapid electron transfer process, which can be attributed to the restoration of the sp^2-hybridized graphitic network during the reduction process and synergistic effects between rGO and NiNPs. The size of the NiNPs, obtained by gamma irradiation, is smaller than 10 nanometers, resulting in an increased electrode/electrolyte contact area and reduced distances for both electronic and ion transport.

4. Conclusion

In summary, we have successfully synthesized rGO–Ni nanocomposites through a one-step process using gamma irradiation. XRD analysis confirmed the reduction of both Ni^{2+} and GO, while TEM images and size distribution histograms indicated that higher absorbed doses resulted in the production of smaller nanoparticles. It is noteworthy that the ionizing radiation technique allows precise size control of nickel nanoparticles through the simple adjustment of the applied radiation dose. XPS analysis indicated that the oxidation of NiNPs occurred exclusively on the rGO surface, while TG curves suggested the presence of NiNPs between the sheets as well.

The electrochemical behavior of both rGO and rGO–Ni revealed a direct correlation between the absorbed doses used in the reduction process and the anodic peak current. Moreover, all modified SPE samples exhibited reduced ΔE and increased average electroactive area compared to the unmodified SPE, indicating enhanced electron transfer capability on the modified electrode surfaces. These findings highlight the potential use of gamma irradiation for synthesizing rGO–Ni nanocomposites for electronic devices.

Author contributions

Raynara M. S. Jacovone: investigation, formal analysis, visualization, and writing – original draft. Miguel Duarte: investigation and formal analysis. Jaqueline J. S. Soares: investigation and formal analysis. Rubens N. Faria: methodology. Rafael H. L. Garcia: formal analysis. Lúcio Angnes: investigation. Solange Kazumi Sakata: conceptualization, methodology, validation, supervision, funding acquisition, and writing – review and editing.

Conflicts of interest

There are no conflicts to declare.

Data availability

Data supporting this study are included within the article and/or data will be available upon request.

Acknowledgements

This work was supported by the National Council for the Improvement of Higher Education (CAPES) and the International Atomic Energy Agency (IAEA) in the framework of the Coordinated Research Project F22070. The authors would like to acknowledge the Material Science and Technology Center (CCTM/IPEN) staff for assistance in acquiring the TEM images. This research used facilities of the Brazilian Nanotechnology National Laboratory (LNNano), part of the Brazilian Centre for Research in Energy and Materials (CNPEM), a private non-profit organization under the supervision of the Brazilian Ministry for Science, Technology, and Innovations (MCTI). The spectroscopy and light scattering staff are acknowledged for their assistance during the experiments XPS 28102.

References

1 Z. Ji, X. Shen, G. Zhu, H. Zhou and A. Yuan, *J. Mater. Chem.*, 2012, **22**, 3471–3477.
2 S. M. Youssry, M. A. Elkodous, R. Kumar, G. Kawamura, W. K. Tan and A. Matsuda, *Electrochim. Acta*, 2023, **463**, 142814.
3 H. Zhang, L. Yang, X. Li, Y. Ping, J. Han, S. Chen and C. He, *Dalton Trans.*, 2024, **53**, 4680–4688.
4 G. B. Pour, H. N. Fard, L. F. Aval and D. Dubal, *Mater. Adv.*, 2023, **4**, 6152–6174.
5 X. Xia, J. Tu, Y. Mai, R. Chen, X. Wang, C. Gu and X. Zhao, *Chem. – Eur. J.*, 2011, **17**, 10898–10905.
6 Y. G. Zhu, G. S. Cao, C. Y. Sun, J. Xie, S. Y. Liu, T. J. Zhu, X. B. Zhao and H. Y. Yang, *RSC Adv.*, 2013, **3**, 19409–19415.
7 A. Sheng, Y. Yang, D. X. Yan, K. Dai, H. Duan, G. Zhao, Y. Liu and Z. M. Li, *Carbon*, 2020, **167**, 530–540.
8 L. Niu, J. Wang, W. Hong, J. Sun, Z. Fan, X. Ye, H. Wang and S. Yang, *Electrochim. Acta*, 2014, **123**, 560–568.
9 D. M. Clifford, C. E. Castano and J. V. Rojas, *Radiat. Phys. Chem.*, 2017, **132**, 52–64.
10 N. E. Zikalala, S. Azizi, F. T. Thema, K. J. Cloete, A. A. Zinatizadeh, T. Mokrani, N. Mketo and M. M. Maaza, *FlatChem*, 2024, **45**, 100662.
11 H. Zhao, Z. Li, N. Zhang, Y. Du, S. Li, L. Shao, D. Gao, X. Han and P. Xu, *RSC Adv.*, 2014, **4**, 30467–30470.

12 Y. Zhang, X. Zhang, H. L. Ma, L. Wang, X. Zeng, L. He, P. Liu, Z. Wang and M. Zhai, *Materials*, 2018, **11**, 2145.
13 W. S. Hummers and R. E. Offerman, *J. Am. Chem. Soc.*, 1958, **80**, 1339.
14 A. N. Geraldes, D. F. Silva, E. S. Pino, J. C. M. Silva, R. F. B. Souza, P. Hammer, E. V. Spinacé, A. O. Neto, M. Linardi and M. C. Santos, *Electrochim. Acta*, 2013, **111**, 455–465.
15 R. Flyunt, W. Knolle, A. Kahnt, A. Prager, A. Lotnyk, J. Malig, D. Guldi and B. Abel, *Int. J. Radiat. Biol.*, 2014, **90**, 486–494.
16 P. Wang, D. Zhang, L. Zhang and Y. Fang, *Chem. Phys. Lett.*, 2013, **556**, 146–150.
17 H. Remita and I. Lampre, *Materials*, 2024, **17**, 364.
18 W. Ostwald, *Phys. Chem.*, 1900, **34**, 495.
19 I. M. Lifshitz and V. V. Slyozov, *Phys. Chem. Solids*, 1961, **19**, 35–50.
20 X. Gao, H. Zhang, E. Guo, F. Yao, Z. Wang and H. Yue, *Microchem. J.*, 2021, **164**, 105979.
21 F. Wang, Y. Liu, Z. Song, Z. Miao and J. Zhao, *Catalysts*, 2021, **11**, 561.
22 M. C. Biesinger, B. P. Payne, L. W. M. Lau, A. Gerson and R. S. C. Smart, *Surf. Interface Anal.*, 2009, **41**, 324–332.
23 R. M. S. Jacovone, J. J. S. Soares, T. S. Sousa, F. R. O. Silva, R. H. L. Garcia, H. N. Nguyen, D. F. Rodrigues and S. K. Sakata, *Energy, Ecol. Environ.*, 2019, **4**, 318–324.
24 S. Cinti, F. Arduini, M. Carbone, L. Sansone, I. Cacciotti, D. Moscone and G. Palleschi, *Electroanalysis*, 2015, **27**, 2230–2238.
25 M. V. Stackelberg, M. Pilgram and V. Toome, *Z. Elektrochem.*, 1953, **57**, 342–350.
26 S. A. Mamuru and N. Jaji, *J. Nanostruct. Chem.*, 2015, **5**, 347–356.
27 W. Huang, S. Ding, Y. Chen, W. Hao, X. Lai, J. Peng, J. Tu, Y. Cao and X. Li, *Sci. Rep.*, 2017, **7**, 1–11.
28 P. Norouzi, A. Karimpour and M. R. Ganjali, *J. Mater. Sci.: Mater. Electron.*, 2019, **30**, 16184–16194.